International Journal of Pharmaceutics 602 (2021) 120664

Contents lists available at ScienceDirect

International Journal of Pharmaceutics

journal homepage: www.elsevier.com/locate/ijpharm

Degradation study on molecules released from laser-based jet injector

Jan Krizek [a,*], Barbora Lavickova [b], Christophe Moser [a,*]

[a] School of Engineering, Laboratory of Applied Photonics Devices, Swiss Federal Institute of Technology in Lausanne (EPFL), Station 17, 1015 Lausanne, Switzerland
[b] School of Engineering, Laboratory of Biological Network Characterisation, Swiss Federal Institute of Technology in Lausanne (EPFL), Station 17, 1015 Lausanne, Switzerland

ARTICLE INFO

Keywords:
Needle-free injection
Jet injection
Laser cavitation
Degradation
Minimally invasive
Drug delivery
Optofluidics

ABSTRACT

Development of needle-free methods to administer injectable therapeutics has been researched for a few decades. We focused our attention on a laser-based jet injection technique where the liquid-jet actuation mechanism is based on optical cavitation. This study investigates the potential damage to therapeutic molecules which are exposed to nanosecond laser pulses in the configuration of a compact laser-based jet injection device. Implementation of a pulsed laser source at 1574 nm wavelength allowed us to generate jets from pure water solutions and circumvent the need to reformulate therapeutics with absorbing dyes. We performed H1-NMR analysis on exposed samples of Lidocaine and δ-Aminolevulinic acid. We made several tests with linear and plasmid DNA to assess the structural integrity and functional potency after ejection with our device. The tests showed no significant degradation or detectable side products, which is promising for further development and eventually clinical applications.

1. Introduction

The needle-free jet injection is a non-contact technique investigated to deliver injectable therapeutics without needles (Mitragotri, 2006). It was initially introduced for mass vaccination programs to avoid contaminated waste from used needles and reduce patients' fear of injection (Weniger and Papania, 2013). Although it has not yet been widely accepted in clinical practice, this approach has multiple advantages: it is contactless, provides better dose control, superior depth and lateral localisation and notably lower collateral damage to the tissue (Arora et al., 2008; Cu et al., 2020; Delrot et al., 2018). Further, it also proved to promote the efficacy of several treatments such as photodynamic therapy (Barolet and Boucher, 2011; Gong et al., 2016; Harris and Pierpoint, 2012; Li et al., 2013), gene therapy (Fargnoli et al., 2016; Horiki et al., 2004; Kunugiza et al., 2006; Sawamura et al., 1999; Taniyama et al., 2012; Walther et al., 2008; Walther et al., 2001) and others (Barolet and Benohanian, 2018; Jones et al., 2019).

The force pushing a liquid out of a nozzle can be generated by releasing mechanical energy from a loaded spring or compressed gas (Weniger and Papania, 2013), piezoelectric element (Arora et al., 2007; Stachowiak et al., 2009; Stachowiak et al., 2007), Lorentz force actuator (McKeage et al., 2018; Taberner et al., 2012), electrical breakdown (Fletcher and Palanker, 2001; Avila et al., 2015) or chemical reaction (Chang et al., 2019; Aran et al., 2017;9.). A relatively new approach employs laser-induced cavitation in liquids as a jet's driving mechanism (Krizek et al., 2020; Krizek et al., 2020; Han and Yoh, 2010; Jang et al., 2014; Park et al., 2012; Berrospe-Rodriguez et al., 2016; Oyarte Gálvez et al., 2019; Oyarte Gálvez et al., 2020; Rodríguez et al., 2017; Tagawa et al., 2013; Rohilla and Marston, 2020; Moradiafrapoli and Marston, 2017; Shangguan et al., 1996). Energy deposition leads to a localised phase transition resulting in bubble generation and its abrupt growth (Vogel and Venugopalan, 2003). The laser-based jet injection is gaining more attention among clinicians as the first device obtained the Ce-MDD certification for use as a medical device in Europe. The device developed by JSK Medical is based on the work of Yoh et al. (Han and Yoh, 2010; Jang et al., 2014; Park et al., 2012) and consists of two compartments. The first one serves as a drug reservoir with a nozzle opening, and the second reservoir contains water to absorb laser light. This way, the laser light does not interact with the drug, so potential damage is excluded. Another promising direction, especially for intradermal injection, is the implementation of laser diodes in a continuous wave emission regime. A relatively low price of such a system can fulfil the need for a portable and widely used needle-free injection device (Berrospe-Rodriguez et al., 2016; Oyarte Gálvez et al., 2019; Oyarte Gálvez et al., 2020; Rodríguez et al., 2017). A new type of highly-focused liquid microjets was proposed for jet injection by Tagawa et al. (Tagawa et al., 2013). Further studies

* Corresponding authors.
E-mail addresses: jan.krizek@epfl.ch (J. Krizek), christophe.moser@epfl.ch (C. Moser).

https://doi.org/10.1016/j.ijpharm.2021.120664
Received 26 November 2020; Received in revised form 16 April 2021; Accepted 26 April 2021
Available online 30 April 2021

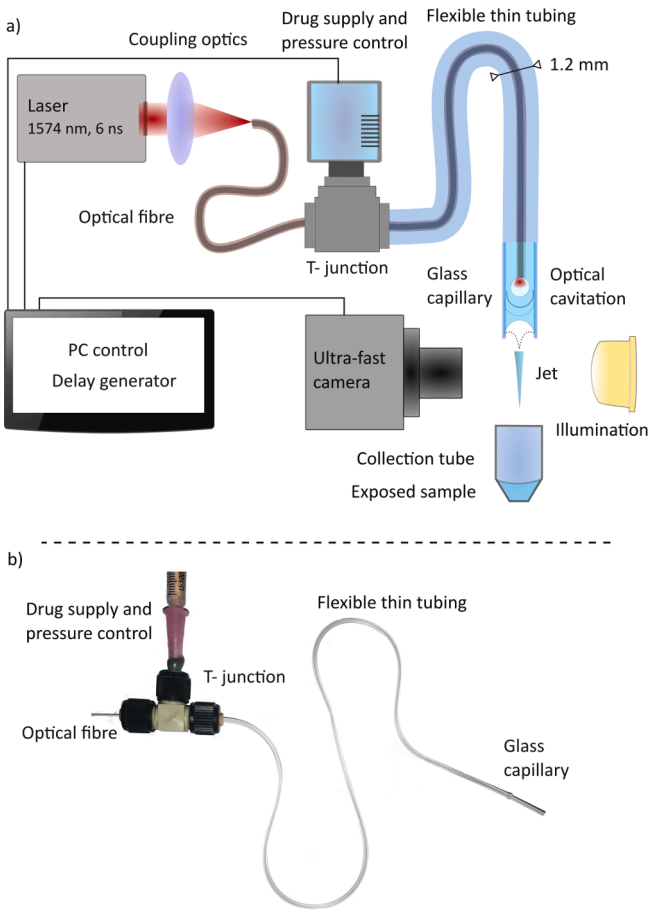

Fig. 1. a) System set-up for the laser-based liquid jet generation and collection of the exposed sample. b) Picture of the laser-based jet injector.

on these jets demonstrated injection into gel phantoms and *ex vivo* injection into the skin (Krizek et al., 2020; Rohilla and Marston, 2020; Kiyama et al., 2019). Laser light represents an exciting alternative because, as opposed to other actuation schemes, it allows the compact size of the end nozzle (Krizek et al., 2020). Hence, it potentially broadens the applications as mentioned above to target intrabody organs in minimally invasive procedures.

Subjecting a drug to direct laser illumination raises concerns about potential damage to the liquid substance, which may be caused by excessive heating or light-induced degradation. To the best of our knowledge, no study has explored drug degradation in this context. It is a large gap of knowledge because if such damage is demonstrated, it would be difficult to translate the technology into clinical practice. In our previous study, we examined the integrity of large biomolecules (rabbit immunoglobulin) (Krizek et al., 2020) and showed, by immunoassay, that even after deposition, they keep their affinity to antibodies. Although this was an encouraging result, the method lacks information about potential side products and providing only qualitative results. The purpose of the present study is to quantitively analyse potential by-products of several compounds resulting from laser light actuation.

For this, we need to collect enough sample volume (>µl), which poses a technological challenge as a single jet contains only ≈10 nL. In this manuscript, we adapted a method for jetting in a repetitive regime from Krizek et al. (Krizek et al., 2020) to reach a sufficient volume of around 10 µL by collecting jets with a frequency of 10 Hz. Moreover, we used a new laser system whose wavelength and pulse energy ($\lambda = 1.57\ \mu m,\ 6\ ns,\ E < 4.5\ mJ$) is capable of producing a bubble without requiring dye additives. It is an essential step for the analysis as the dye can distort our results and for the clinical use where the drug's reformulation is not favourable. We used proton nuclear magnetic resonance (H^1-NMR) to study the degradation of therapeutic molecules, such as Lidocaine (Patakfalvi and Benohanian, 2014) or δ-Aminolevulinic acid (Agostinis et al., 2011). H^1-NMR analysis did not show any detectable degradation products on heat-sensitive and photosensitive molecules. Considering the attractive use of this technology for gene delivery, we examined the effect of our device on linear and plasmid DNA molecules. Several tests challenging the structure and functionality of DNA molecules are showing no exceptional degradation products or side effects after processing with a laser-based jet injection device. This positive outcome is promising for pre-clinical and clinical studies with laser-based jet injection devices.

2. Methods

2.1. Set-up

We used a similar experimental set-up as in our previous study (Krizek et al., 2020). The experimental set-up is depicted in Fig. 1. Liquid microjets are actuated by optical cavitation on the tip of an optical fibre (105 µm, ThorLabs, FG105LCA). The end part of the fibre is stripped from the coating (250 µm) so that the end facet can be cleaved. The larger diameter of the coating facilitates the positioning of the fibre towards the axis of the capillary. The fibre is located in the centre of a round-shaped glass capillary with an inner diameter of 300 µm and 1.2 mm outer diameter. The capillary is attached to a flexible Teflon tubing and plugged into a T-junction (Upchurch, Scientific MicroTees) which

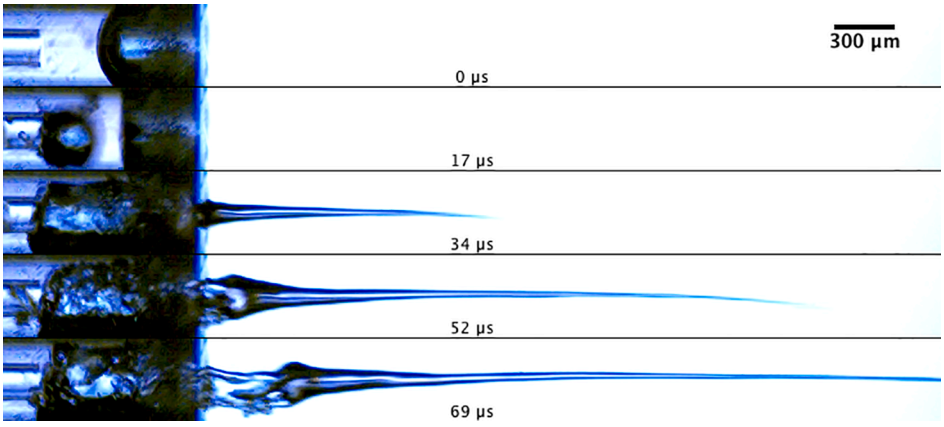

Fig. 2. Pure DI water jet. Image sequence from the ultrafast camera $v_{jet} = 98$ m/s, $E_{laser} = 2.2$ mJ. NIR absorption band of water allows the generation of jet without dye additive; hence there is no need to reformulate drug before its use.

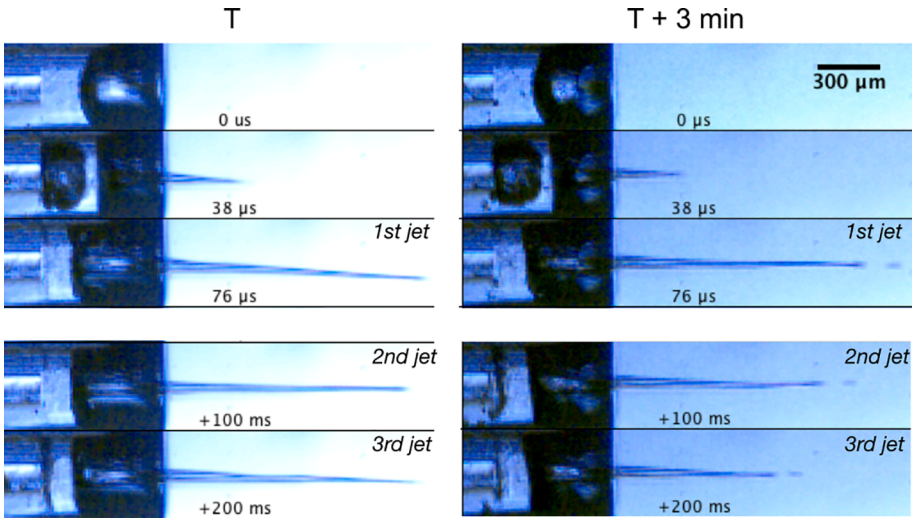

Fig. 3. Jets of 4% Lidocaine in repetitive regime with the velocity around 45 m/s, 10 Hz. Two sequences of 3 jets captured with 3 min delay to each other in one continuous jetting cycle. Left: Jet sequence recorded at the time T, Right: Jet sequence was taken at the time T + 3 min.

connects the fibre with a drug supply and a pressure control unit (Low-Pressure Syringe Pump neMESYS 290 N, CETONI) operated by a computer. A laser (Falcon Lumibird, $\lambda = 1.57\ \mu m,\ 6\ ns,\ E < 4.5\ mJ$) is coupled into the optical fibre. It is essential to achieve a high coupling efficiency to maximise the energy at the fibre tip and minimise the probability of laser-induced damage to the fibre input. The energy value noted in this manuscript is measured at the distal end of the fibre by an energy meter (Thorlabs, ES111C). The jet generation and its parameters are monitored by an ultra-fast camera (Vision Research, Phantom Miro M310). Laser action and the camera are synchronised with a delay generator (Berkley Nucleonics, Model 577). The liquid jets (exposed sample) are ejected and collected in a tube. The total collected volume is the result of multiple jets. We equipped the illumination system with a coloured glass filter (FGB37S, ThorLabs) filtering the IR spectrum to protect the sample from heating during the sample collection.

2.2. Laser-induced microjets

Highly focused microjets can be generated from axisymmetric capillaries with the actuation mechanism based on laser-induced liquid cavitation (Tagawa et al., 2012). The sequence of the jet generation is depicted in Fig. 2. The fluid is pushed from the tube by the growing bubble. The liquid/air meniscus curvature causes the pressure gradient, which is oriented towards the centre and enables further acceleration into a needle-like shape. Variation in the meniscus shape or decentralisation of the fibre position may cause minor variation in the jet shape, like slight inclination of the jet tip seen in Fig. 2. More information on the jet parameters and soft material penetration characteristic can be found in (Krizek et al., 2020; Krizek et al., 2020; Kiyama et al., 2019; Tagawa et al., 2013; Rohilla and Marston, 2020; Moradiafrapoli and Marston, 2017).

2.3. Laser system ($\lambda = 1.57\ \mu m,\ 6\ ns,\ < 4.5\ mJ$)

This section explains the choice of the laser Falcon Lumibird ($\lambda = 1.57\ \mu m,\ 6\ ns,\ E < 4.5\ mJ$). The wavelength of the laser is close to the first infra-red absorption overtone of water, yielding a relatively high absorption coefficient around 9 cm^{-1} (Hale and Querry, 1973). Even a better choice would be a system with $\lambda = 1.45\ \mu m$, where the absorption reaches 28.8 cm^{-1}. However, such a system is currently not available on the market. Simultaneously, this wavelength is known to have the lowest attenuation in silica-based optical fibres hence exhibiting the highest damage threshold (Keiser et al., 2014). Delivering enough energy is essential to create cavitation and eject liquids from a pure water solution with no additives. It is a necessary step towards a potential clinical use as there is no need for further modification of the drug with a dye that facilitated laser absorption, such as was used in previous studies (Krizek et al., 2020; Krizek et al., 2020; Tagawa et al., 2013). Moreover, this laser system is relatively small in size ($144 \times 64 \times 38\ mm$), lightweight, and can be powered by a battery and thus even portable or adaptable into a desk-top sized system.

2.4. Repetitive regime and operation condition

A single jet volume in our configuration is about 10 nL which is too little to run analytical tests. The target volume of the exposed sample is in the range of 10 µL; therefore, we need to collect at least 10^3 jets. To do this efficiently, we used the repetitive jet ejection regime reported in (Krizek et al., 2020). By careful adjustment of the flow rate together with the laser pulse energy and the repetition rate, we were able to achieve stable jetting. As an example, we show a sequence of three jets of Lidocaine solution from one continuous jetting cycle with 3 min delay between each other. The jetting parameters are in Fig. 3, showing jets with velocity around 45 m/s, jet repetition rate 10 Hz and laser pulse energy of 2.25 mJ. The measured speed of single jets was varying within 10%.

Rohilla and Marston (Rohilla and Marston, 2020) pointed out that in some instances, the bubble gets trapped in the nozzle and then the sequence has to be stopped and readjusted. A set-up with a short distance between the fibre tip and meniscus interface is more resistant to this effect. However, in some cases, it happened, and it indeed poses a practical limit to the current setting as we rely on the visual feedback from the camera because the uncontrolled leak is unfavourable. From our experience, once the system is defined, there is no need to monitor the jet with the ultrafast camera, but only the interface's position, which could be forced, e.g. by a microfluidic stop valve.

Clinically relevant doses are 10–100 µL for DNA vaccination (Chang et al., 2019), 10 s of µL for tumour gene therapy (Walther et al., 2008; Walther et al., 2005), 0.4 mL for photodynamic therapy (Barolet and Boucher, 2011; Gong et al., 2016; Harris and Pierpoint, 2012; Li et al., 2013), 0.1–0.5 mL cardiac gene therapy (Fargnoli et al., 2014), 10 – 100 µL per site for lidocaine anaesthesia (Barolet and Benohanian, 2018) to treat dermatological conditions. This clearly points out that the dose rate should be augmented in future design. There are several possible strategies: an increased repetition rate, parallel nozzle design for simultaneous injections, higher concentration of the therapeutic molecule

thanks to the extended range of injectable viscosity (Delrot et al., 2016).

2.5. Degradation effects

2.5.1. Thermal effects

The laser interaction with the fluid generates the driving force for the jet acceleration. Thermal side effects are a source of concern, because absorbed optical energy is transformed into heat. A common strategy to mitigate heat damage is selecting short pulse duration and minimising heat diffusion (Vogel and Venugopalan, 2003). For *ns* laser pulses, the high energy deposition rate can cause so-called thermal confinement, which in other words means that the heat does not escape out of the irradiated region during the time of deposition. This happens when the pulse duration is shorter than the heat diffusion time t_{th}:

$$t_{th} < \frac{\delta^2}{4\kappa} = 4.8\ ms \tag{1}$$

Where δ is the smallest dimension of the irradiated volume (in this case, the fibre core radius = 52.5 μm; for a highly absorptive medium it could be optical penetration depth) and κ is thermal diffusivity of water ($\kappa = 1.44 \times 10^{-3}\ cm^2/s$).

Moreover, stress confinement happens when the pulse is shorter than the stress relaxation time t_{ac}:

$$t_{ac} < \frac{\delta}{c} = 35\ ns \tag{2}$$

Where δ is the smallest dimension of the irradiated volume and c is the speed of sound in the medium (1500 m/s). Then in the vicinity of the fibre tip, the pressure is temporarily built up, and boiling can occur at temperatures below 100 °C (Frenz et al., 1998; Paltauf et al., 1998).

Considering there is no heat exchange from irradiated volume ($\tau_{pulse} < t_{th}$), we can calculate the temperature rise ΔT as following:

$$\Delta T = \frac{\alpha F}{\rho c_v} \tag{3}$$

Where α stands for the linear absorption, F for the fluence of the laser pulse, ρ is the density of the fluid, c_v is the specific heat capacity. Typical values for our system are $\alpha = 9.34\ cm^{-1}$, $F = 28\ J\ cm^{-2}$ (for the pulse of 2.4 mJ), $\rho = 1\ g\ cm^{-3}$, $c_v = 4.2\ J\ K^{-1}g^{-1}$ which gives the peak value of $\Delta T = 62°$. This temperature change alone would not lead to the vapour bubble initiation, therefore we assume that built-up pressure on the fibre tip leads to the decreased limit for bubble nucleation similar to (Frenz et al., 1998; Paltauf et al., 1998).

Linear absorption of the water for the given laser radiation is $\alpha = 9.34\ cm^{-1}$ which predicts that most of the energy is not used and radiated out of the system. Along the beam path, the fluid is heated, which for the illumination scheme with 105 μm fibre means that almost 1/8 of the total sample is heated. The average temperature rise in this volume is 56 °C, and if we consider perfect mixing with the whole liquid shortly after heating due to the bubble cavitation and jet generation (<30 μs), the average temperature rise of the entire ejected volume is only around 7 °C.

This is well in agreement with results from the study of Quinto-Su et al. (Quinto-Su et al., 2014) who measured thermal effects accompanied to the ns laser-induced cavitation. In their observation, the temperature rise is only moderate (<12.8 °C) and highly localised.

2.5.2. Photo-induced effects

A photo-initiated chemical reaction can cause another potential damage to the therapeutics. Light can provide activation energy to initiate a chemical reaction which would result in the production of unfavourable side products. The extent of this effect is given by the ability of molecules to absorb light of a specific wavelength. From the light radiation spectrum, UV photons have the highest energy and could initiate chemical changes more effectively than light with a longer wavelength.

Side products in photosensitive materials were reported in droplets generated by Laser direct writing technique (Kattamis et al., 2009). The droplet generation scheme is different: the UV laser light illuminates a 6 μm thin liquid layer; hence, a large portion of the sample is exposed, and the whole volume is in close vicinity to the cavitation site. Moreover, UV photons have high energy and could initiate chemical changes more effectively than light with a longer wavelength.

Photo-induced chemical reactions for nanosecond laser pulses in the near-infrared spectrum has not been reported. In general, photons in NIR have low energy and are not interacting directly with the covalent bonds of molecules. However, they can interact with vibration states of molecules and cause localised heating which might lead to some structural changes such as unfolding larger protein molecules (Jones et al., 1993).

2.5.3. Mechanical stress effects

The disintegration of the molecular structure due to mechanical stress is a problem mainly for larger molecules like proteins or nucleic acids. In the case of needle-free injection devices, this concern is based on the shear pressure during the jet generation and upon impact. Later studies provided an argument that no such degradation on peptides and proteins are present after processing with a spring-actuated needle-free injection device (Benedek et al., 2005). Another study (Hogan et al., 2006) confirms that result by *in-vivo* efficacy test, showing that therapeutic enzymes sustain their function after administration by Lorenz-force actuated needle-free injector. A very susceptible substance to shear stress is a plasmid DNA vector used for gene therapy (Catanese et al., 2012). Walther et al. (Walther et al., 2001; Walther et al., 2002; Cartier et al., 2000) showed that using the air-powered actuation pressure higher than 2.5 bar leads to topology changes in DNA plasmids. Later studies showed that such damage is not a limiting factor for efficient *in vivo* gene transfer (Walther et al., 2008; Walther et al., 2005), nevertheless, the loss of 20–40% of therapeutic plasmid has to be accounted (Walther et al., 2001).

The positive feature of our laser-based jet injector is the inviscid character of the jet (Peters et al., 2013), which is not in contact with the nozzle wall and therefore, the substrate does not experience shear stress during the jetting action. However, another source of mechanical stress may occur due to the photoacoustic waves, which are exited in liquids by short laser pulses (Paltauf et al., 1998). This effect occurs only in conditions of the stress confinement (*Equation (2)*), and considering the parameters of our system, we have to take this effect into account. The high-amplitude peak pressure (≈10^7 Pa) (Paltauf and Schmidt-Kloiber, 1996) leads to a cloud of cavitation bubbles along the axis of the fibre and takes place before the main vapour bubble is generated (<1 μs) (Paltauf et al., 1998). This cavitation cloud is similar in nature to bubbles generated during sonication, which has been demonstrated to have a damaging effect on plasmid DNA when exposed for an extended time. Unfortunately, our imaging system does not have the proper time resolution to study this phenomenon in detail.

2.6. Small molecules preparation protocol

5-Aminolevulinic acid hydrochloride (Sigma-Aldrich Chemie GmbH) was mixed with DI water to a concentration of 100 mg/mL. The solution was further split into three separate samples – one was directly collected for NMR analysis; the second was exposed with the laser-actuated jet injector, and the last was subjected to a forced degradation. Jets were generated in the repetitive regime with laser pulse energy 2.75 mJ and 10 Hz. Forced degradation consisted of heating the sample to 90 °C for 10 min and simultaneous exposition to a bright light source (LED diode LZC-00CW0R, Led Engin®, I = 50 mW/cm^2 at the sample position plane). 10 μL of each sample was diluted in 500 μL of D_2O (Sigma-Aldrich Chemie GmbH) and poured into a NMR tube (Wilmad WG-

1228–7). NMR analysis was done within one hour since the initial solution preparation and samples were kept in the dark and cooled by chopped ice.

Lidocaine hydrochloride (Sigma-Aldrich Chemie GmbH) was mixed with DI water to a concentration of 40 mg/mL. The solution was further split into two separate samples – one was directly collected for NMR analysis, the second was exposed by the laser-actuated jet injector. Jets were generated in the repetitive regime with laser pulse energy 2.75 mJ and 10 Hz. 10 μL of each sample was diluted in 500 μL of D_2O (Sigma-Aldrich Chemie GmbH) and poured into a NMR tube (Wilmad WG-1228-7).

2.7. DNA preparation protocol

pET21a(+)-Histag-Citrine plasmids and *pET21a(+)-Histag-mCherry* were used in the study obtained from Addgene (Addgene plasmid # 70718, # 70719) (Niederholtmeyer et al., 2015). Linear template DNA was amplified from *pET21a(+)-Histag-Citrine* plasmid by PCR with primers: 5′ GCGTCCGGCGTAGAGGATC 3′ and 5′ GCGTCCCATTCGCCAATCCG 3′. The plasmid *pET21a(+)-Histag-mCherry* was used for the plasmid degradation study. The plasmid and linear template DNA were purified using ZymoPURE Plasmid Miniprep and DNA Clean and Concentrator-25 (Zymo Research), respectively. DNA was eluted in nuclease-free water instead of elution buffer. The DNA samples were further split into two separate samples – one was used for analysis, the second was exposed by the laser-actuated jet injector. All the samples were stored at −20 °C.

2.8. DNA degradation study protocols

DNA concentration was measured by NanoDrop™ One (Thermo Scientific). Separation of DNA by size was done by agarose gel electrophoresis. For agarose gel electrophoresis, 1.75 μL of DNA solution was loaded into a 1% agarose gel. For restriction digest, 1.5 μL of plasmid DNA was digested in NEBuffer 3.1 buffer with 2 U of BamHI-HF (NEB Inc.) for 20 min at 37 °C, 1.35 μL of the DNA solution were loaded into an agarose gel. Electrophoresis parameters were the following: gels were run at 100 W for 40 min unless otherwise stated, stained with SYBR Safe DNA Gel Stain (Thermo Scientific) and image with Benchtop 3UV transilluminator (UVP) and EL Logic 100 imaging system and analysed with ImageJ. Additionally, the DNA samples were amplified by PCR, purified as described above and send for Sanger Sequencing (Microsynt).

We performed a forced degradation of DNA by using a sonication bath. 150 μL of DNA solution was sonicated on ice using a probe sonicator (Vibra cell 75186, probe tip diameter: 3 mm) with 50% or 20% amplitude for linear or plasmid DNA, respectively.

Plasmid samples were 300 × diluted in water and transformed into 15 uL High-Efficiency 5-alpha Competent E. coli (NEB Inc.) based on a standard protocol and mixed with 100 μL of SOC media. 100 μL of the suspended cells were directly plated on an LB agar plate and incubated at 37 °C for 24 h. Transformed colonies were picked up from to the plate and send from Ecoli NightSeq® sequencing (Microsynt).

Cell-free expression reactions were performed in a reconstituted transcription-translation system (PURE system) as previously described in (Lavickova and Maerkl, 2019). PURE reactions (5 μL) were established by mixing 2 μL of 2.5 × energy solution, 0.9 μL of 10 μM ribosomes (final concentration: 1.8 μM), 0.65 μL of OnePot PURE and 0.15 μL of DNA template. The mixtures were brought to a final volume of 5 μL with the addition of water and incubated at 37 °C at constant shaking for 3.5 h, and measured (excitations: 425, 475, 585 nm; emission: 475, 530, 610 nm for cerulean, citrine, mCherry, respectively) on a SynergyMX plate reader (BioTek).

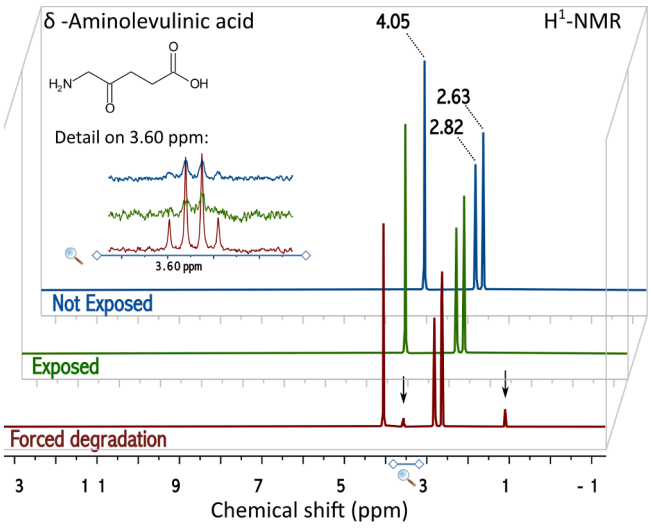

Fig. 4. H^1-NMR spectra of δ-Aminolevulinic acid hydrochloride.

3. Experiments & results

3.1. Stability of small drug molecules

The stability and potential degradation of small molecules are assessed by a proton nuclear magnetic resonance (H^1 MNR, Bruker Avance III 400 MHz NMR spectrometer). It is a standard technique used to identify and characterise degradation products in pharmacy (Maggio et al., 2014). The analysis gives a simple parameter – NMR chemical shift, which yields information about the chemical environment, and it is unique for each compound (Maggio et al., 2014). Comparing the intact drug sample with the exposed one can identify structural changes on a molecular level.

3.1.1. δ -Aminolevulinic acid

δ-Aminolevulinic acid (ALA) is being studied as an agent for photodynamic therapy (PDT) in numerous types of cancer (Agostinis et al., 2011) or treating infections (Harris and Pierpoint, 2012). Jet injectors have been clinically implemented to facilitate otherwise low ALA penetrability through the skin to treat dermatological cancer conditions (Barolet and Boucher, 2011; Gong et al., 2016; Harris and Pierpoint, 2012; Li et al., 2013). The aqueous solution of ALA is thermally sensitive, and even under room temperature, it undergoes degradation of more than 10% within a few hours (Elfsson et al., 1999).

The results of the analysis can be seen in Fig. 4. A spectral signature of a non-exposed sample is the reference (blue line). Compared to the sample exposed by the laser-based jet generator (green line), we do not observe any changes; hence there is no detectable degradational product. On the other hand, looking at the spectra of the forced degradation sample (red line), we see additional peaks that suggest molecular structure changes in the solution. The new peak at 3.58 might point to previously observed degradation product 2,5-dicarboxyethyl-3,6-dihydropyrazine in the reference (Bunke et al., 2000). Looking closely at the region of this peak, we can observe that this signal is present even for *not-exposed* and *exposed* sample. However, the signal-to-noise ratio is lower than 10, which is considered the method's detection limit. For this particular measurement, it means that the concentration of the biproduct for *exposed and not exposed* is lower than 2%. The molecule of 5-ALA is sensitive, so we can hypothesise that the minor degradation happens during the sample handling.

3.1.2. Lidocaine

Lidocaine is a medication used to numb tissue in a specific area. It is administered topically in the form of a gel or as a local injection. Often, it

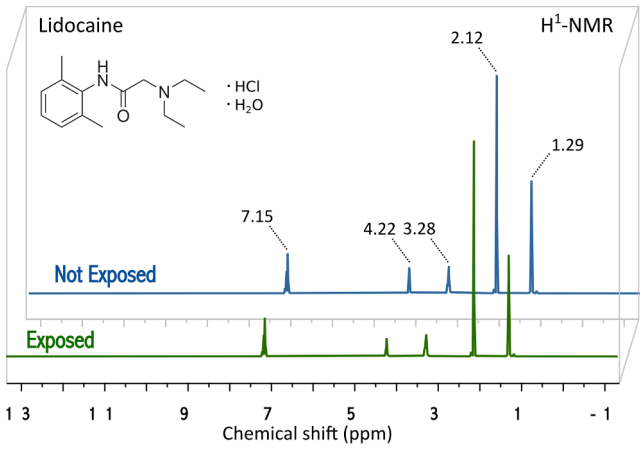

Fig. 5. H^1-NMR spectra of Lidocaine hydrochloride.

has to be applied to a tissue that is already affected, and needle injection then presents an additional source of distress for patients. The jet injection technology can then offer an alternative, less traumatic solution (Patakfalvi and Benohanian, 2014). Lidocaine HCl is very stable against severe heat and light conditions (Kadioglu et al., 2013); the motivation to do the test is driven by a high application potential. Results from the NMR analysis depicted in Fig. 5 suggests no detectable degradation during the process of laser-assisted jetting.

3.2. Stability of DNA

Gene therapy is a promising treatment option for a wide range of human disorders (Dunbar et al., 2018;359.). Naturally, transfection of foreign DNA molecules through a cellular barrier is problematic, which protects us from genetic contamination and helps to preserve our genomic information. Needle-free injection techniques were used both *in vivo* and *in vitro* to facilitate cellular uptake of DNA-based therapeutics (Fargnoli et al., 2016; Horiki et al., 2004; Kunugiza et al., 2006; Sawamura et al., 1999; Taniyama et al., 2012; Walther et al., 2008; Walther et al., 2001). To assess the viability of DNA delivery via laser-based jet injection, we compared exposed samples with the structure of linear and plasmid DNA when subjected to this method, and compared the processed samples with samples subjected to the forced degradation by sonication and thermal heating.

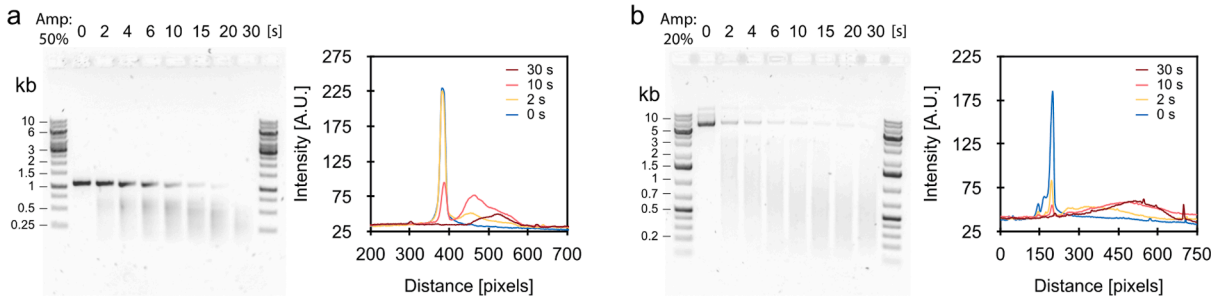

Fig. 6. Forced degradation of linear and plasmid DNA by sonication for different time intervals. A) Agarose gel electrophoresis of the sonicated linear template DNA. The corresponding intensity profiles derived from the gel analysis are plotted as a function of the distance from the top of the gel for the different time intervals. We observe a decrease in the intensity of the 1 kb band due to DNA shearing and smear appearance due to the formation of various lengths of DNA fragments. The time point zero represents the untreated sample. Amplitude (Amp) 50% was used to degrade the linear DNA. B) Agarose gel electrophoresis of the sonicated plasmid DNA. The corresponding intensity profiles derived from the gel analysis are plotted as a function of the distance from the top of the gel for the different sonication time intervals. The band at 6 kb shows the supercoiled (SR) form of the plasmid, while the > 10 kb band shows the relaxed (R) state, and the smear below is a result of the formation of various lengths of DNA fragments. The time point zero represents the untreated sample. Amplitude (Amp) 20% was used to degrade the plasmid DNA.

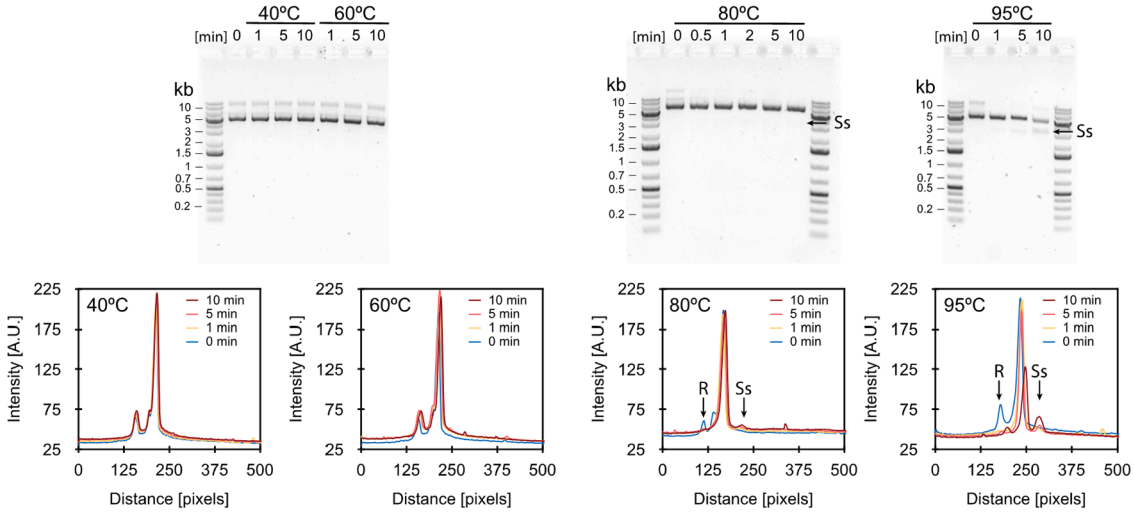

Fig. 7. Forced degradation of plasmid DNA at various temperatures (40 °C, 60 °C, 80 °C, 95 °C) and different time intervals. Agarose gel electrophoresis of the heated plasmid DNA, the band at 6 kb shows the supercoiled (SR) form of the plasmid, while the > 10 kb band shows the relaxed (R) state and the band at 3 kb represents the single-strand (Ss) plasmid DNA (black arrows indicate Ss form). Below are shown intensity profiles, derived from the gel analysis and plotted, as a function of the distance from the top of the gel for the different time intervals at various temperatures. The black arrows indicate the band for the disappearing R form of a plasmid and appearing Ss form. The time point zero represents the unheated sample.

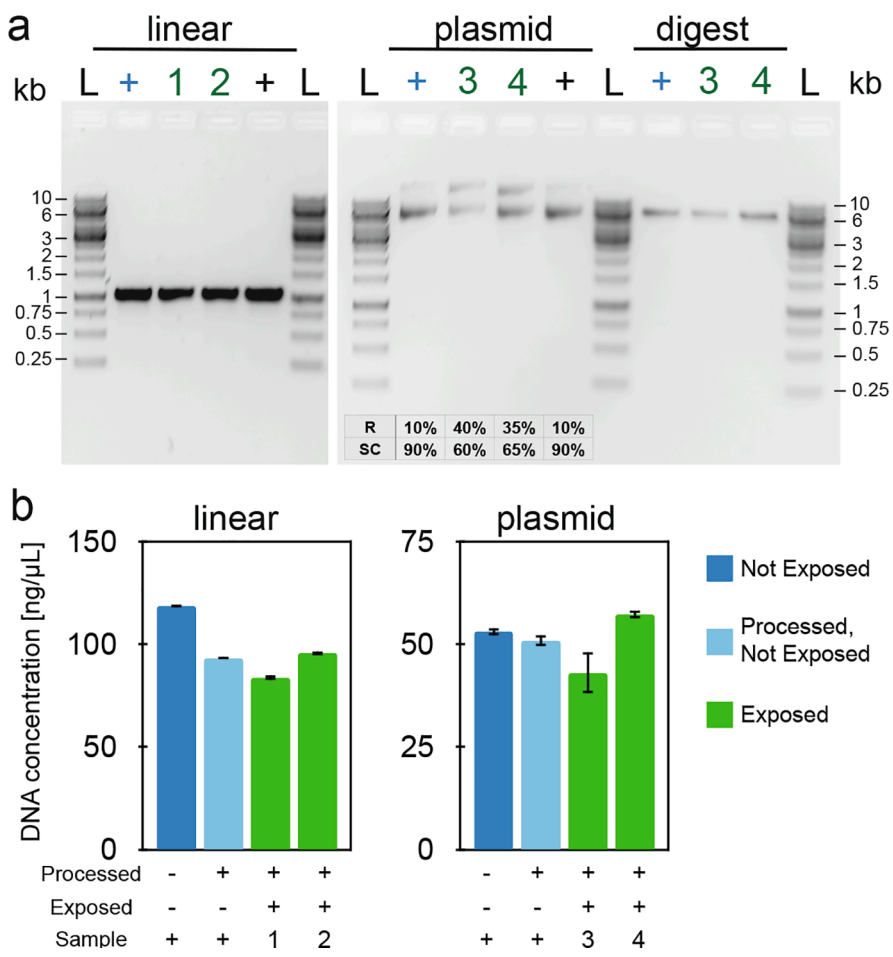

Fig. 8. Degradation of the linear template and plasmid DNA. a) Agarose gel electrophoresis of linear template DNA (1 kb, lanes 2–5). Agarose gel electrophoresis of plasmid DNA (lanes 8–11), the band at 6 kb shows the supercoiled (SC) form of the plasmid, while the > 10 kb band shows the relaxed (R) state of the plasmid. A table below the plasmid lanes (8–11) shows the overall intensities derived from the gel analysis for the different plasmid forms (R, SC) of the corresponding lanes. Agarose gel electrophoresis of plasmid DNA fragments cut by digestion (lanes 13–15). The circular plasmid DNA was digested by the BamHI restriction enzyme to form a single linear DNA fragment instead of more fragments if it had been degraded prior. b) DNA concentration measured before (not exposed) and after passing through a capillary without (processed) or with jet generation (exposed). Data are shown as mean ± s.d. (n = 3, technical replicates). The non-exposed sample is marked as +, linear samples are numbered 1 and 2, and plasmid samples 3 and 4.

3.2.1. Structural integrity of DNA

To assess any structural changes during mechanical and thermal stress, we used agarose gel electrophoresis. Implementing this technique allowed us to separate DNA fragments by length and visualise the DNA samples.

3.2.1.1. Forced degradation of DNA by mechanical stress. We observe that even short and low energy sonication cycles led to visible DNA shearing, apparent from the decrease in intensity of the expected DNA band and the formation of a smear due to the generation of random DNA fragments (Fig. 6).

3.2.1.2. Forced degradation of DNA by thermal stress. In the controlled sample degradation by heating (Fig. 7), a lower amount of DNA degradation was observed than for sonication. For temperatures below 80 °C, we did not observe any degradation or change in plasmid conformation. Temperatures above 80 °C appear to introduce single-stranded plasmid molecules, mainly due to denaturation of the plasmid's relaxed form. When the sample was heated for 10 min at 95 °C, we also saw a transition from supercoiled plasmid to the relaxed form and then further to single-stranded conformation.

3.2.1.3. Analysis of the exposed DNA. We analysed the structure of the exposed DNA samples by agarose gel electrophoresis (Fig. 8a). We compared them to DNA samples subjected to forced degradation by sonication (Fig. 6) and temperature (Fig. 7) to assess if our method might generate similar degraded products. This analysis shows that the laser exposition and jet generation did not induce DNA shearing and that neither the linear nor the plasmid DNA samples suffered significant structural degradation (Sarker et al., 2019; Wu et al., 2016). As in the case of DNA shearing after sonication, we did not see these temperature-induced changes in the sample after jet generation, indicating that sample heating is either not significant or is only too transient (ns) to cause these changes.

However, we observed conformational changes for the undigested plasmid sample (Fig. 8a plasmid). The band at 6 kb shows the supercoiled form of the plasmid, while the > 10 kb band shows the relaxed state of the plasmid (Nguyen and Elimelech, 2007). The intensity increase for the higher band from 10% in not-exposed to 35–40% in exposed samples indicates the formation of the relaxed form of the plasmid. This relaxation could have two sources – thermal or mechanical. As the jet generation is in principle inviscid, we hypothesise that this relaxation may be caused by the cavitation bubble cloud present before the vapour bubble, as discussed in Section 3.4.3. Mechanical induced effects. The damaging effect of this short lasted bubble cloud (<1 µs) would be similar to sonication. However, we could not confirm the root of the structural relaxation, as the energy introduced to the system by sonication is in the *J* range and in order of *s*, and the mechanical energy induced by laser radiation is in the *µJ* range and time order of 100 ns. Nevertheless, compared to other methods like nebulisation, we did not see the significant degradation and adverse effect on the subsequent use of the plasmid (Catanese et al., 2012; Lentz et al., 2005).

Moreover, to confirm that the plasmid sample is not forming a cut-linearised form, we performed restriction digestion. In this process, a sequence-specific part of the plasmid DNA is cut, leading to a linear fragment formation. As expected, the sample digestion led to a single length DNA fragment formation (Fig. 8a digest). As opposed to the case

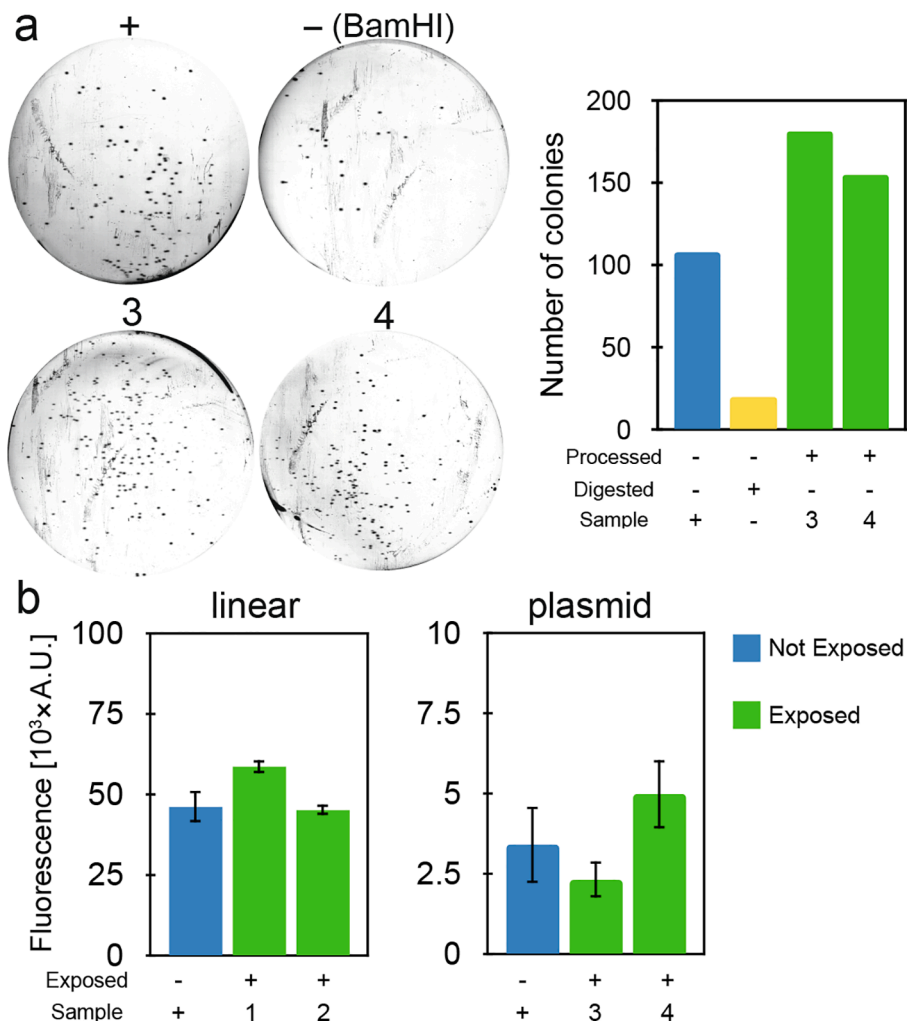

Fig. 9. Degradation of the linear template and plasmid DNA. a) LB agar plates of E. coli 5-alpha cells transformed with the plasmid samples form Fig. 6., exposed (n°3, n°4), not-exposed (+), and digested plasmid samples (–(BamHI)). The cells were grown under selective conditions for ampicillin. The viable, resistant colonies represent bacteria successfully transformed with circular form plasmid containing ampicillin resistance. b) In vitro expression of fluorescence proteins from the different DNA templates. Linear template DNA was coding for YFP (yellow fluorescent protein) and plasmid DNA for mCherry fluorescent protein. An increase in the corresponding fluorescence demonstrates the production of recombinant proteins from the supplied DNA using biomolecular translation machinery extracted from cells. Data are shown as mean ± s.d. (n = 3, technical replicates). The non-exposed sample is marked as +, linear samples are numbered 1 and 2, and plasmid samples 3 and 4.

where the plasmid DNA would be already cut by other causes, which would lead to the formation of multiple linear strands.

3.2.2. DNA concentration

DNA concentration measurements showed a loss of around 25% linear template and 5% plasmid DNA (Fig. 8b). The loss is in agreement with samples processed through the capillary without the laser exposition and jet generation. Therefore, we contribute this loss to the sample handling and absorbance to surfaces, not degradation due to jet formation.

3.2.3. DNA sequencing

To ensure that the DNA was not modified, we amplified all the DNA samples by PCR and sent samples for Sanger sequencing (Microsynt AS). This allowed us to analyse the DNA sequence and determine if there are any mutation, i.e. alternations in the order of the incorporated nucleotides (adenine, guanine, cytosine, and thymine), in the DNA strand. We did not observe any mutation in the fluorescence genes (Data from sequencing are shown in the supplementary table) for the amplified samples.

3.2.4. DNA bacterial transformation with plasmids DNA

To verify that the plasmid DNA preserves its function after the laser-based jetting process, we carried out *E. coli* transformations (Fig. 9a). Uptake of the plasmid DNA by bacteria and following growth and colony formation is conditioned by the correct plasmid function, which is also associated with its structural integrity. Transformations of the exposed products into *E. coli* successfully resulted in a large number of colonies similar to the positive not-exposed sample (Fig. 9a n°3,n°4 exposed: compare to + not-exposed; the graph represents quantitative analysis). In contrast, almost no background colonies were obtained when the sample was digested with BamHI as a negative control (Fig. 9a upper right plate). We sequenced two colonies from each plate to confirm that the transformed plasmids did not contain mutations in the gene coding for the fluorescent protein. We did not observe any mutation in the gene (Data from sequencing are shown in a supplementary table).

3.2.5. In-vitro protein synthesis

Cell-free expression reactions, i.e. production of protein using the biological machinery without the use of living cell, were performed in a reconstituted transcription-translation system (PURE system) as previously described in (Catanese et al., 2012). The fluorescent protein production demonstrated that the exposed DNA could be used by the transcription-translation machinery and generate function protein (Fig. 9b). Contrary to that, degraded or defective DNA could not be transcribed to RNA and subsequently translation to the fluorescent protein. Slight variations in the final fluorescent protein concentration among the samples are probably due to the varying DNA input we did not control.

4. Conclusion

This study explores the potential degradation of products obtained using a custom-built pulsed *ns* laser jet injector (Krizek et al., 2020). We

adapted the device to collect enough sample and employed a new laser system to process pure drug formulations without any additives. Nuclear magnetic resonance spectra show no degradational product on exposed samples of Lidocaine and δ-Aminolevulinic acid. Assessment on the structural integrity of DNA molecules was benchmarked by several tests, including an agarose gel electrophoresis and gene sequencing. We also tested the DNA functionality by *E. coli* transformation and *in vitro* fluorescent proteins expression. All of these showed encouraging results and hence rendered this novel device potentially useful in various therapies. Foreseen applications include anaesthesia (Lidocaine), photodynamic therapy (5-ALA) or gene therapy (DNA). An appealing aspect of this device is the compact size of the end nozzle (long and thin) to reach inaccessible inner body locations.

5. Contribution

JK built the device, collected samples, prepared samples, ran the analysis with Lidocaine and 5-ALA and wrote the manuscript. BL prepared samples and made the analysis of DNA, and wrote related sections of the manuscript. CM supervised the work and revised the manuscript.

Declaration of Competing Interest

The authors declare that they have no known competing financial interests or personal relationships that could have appeared to influence the work reported in this paper.

Acknowledgements

JK acknowledges Dr Aurélien Bornet for his help with NMR analysis. The authors appreciate discussion with Laura Grasemann and Gregoire Michielin on DNA analysis. BL acknowledges Sebastian Maerkl, who provides the facility where DNA tests were done. All authors acknowledge the host institution and funding provided by the EPFL.

Appendix A. Supplementary data

Supplementary data to this article can be found online at https://doi.org/10.1016/j.ijpharm.2021.120664.

References

Mitragotri, S., 2006. Current status and future prospects of needle-free liquid jet injectors. Nat. Rev. Drug Discov. 5, 543–548. https://doi.org/10.1038/nrd2076.
Weniger, B.G., Papania, M.J., 2013. Alternative vaccine delivery methods. Vaccines 1200–1231. https://doi.org/10.1016/B978-1-4557-0090-5.00063-X.
Arora, A., Prausnitz, M.R., Mitragotri, S., 2008. Micro-scale devices for transdermal drug delivery. Int. J. Pharm. 364, 227–236. https://doi.org/10.1016/j.ijpharm.2008.08.032.
Cu, K., Bansal, R., Mitragotri, S., Fernandez, R.D., 2020. Delivery Strategies for Skin: Comparison of Nanoliter Jets, Needles and Topical Solutions. Ann. Biomed. Eng. 48, 2028–2039. https://doi.org/10.1007/s10439-019-02383-1.
Delrot, P., Hauser, S.P., Krizek, J., Moser, C., 2018. Depth-controlled laser-induced jet injection for direct three-dimensional liquid delivery. Appl. Phys. A 124, 616. https://doi.org/10.1007/s00339-018-2030-6.
Barolet, D., Boucher, A., 2011. No-needle jet intradermal aminolevulinic Acid photodynamic therapy for recurrent nodular Basal cell carcinoma of the nose: a case report. J. Skin Cancer 2011, 790509. https://doi.org/10.1155/2011/790509.
Gong, Y., Labh, S., Jin, Y., Diao, H.-Y., Li, X.-L., Liu, Z.-Y., et al., 2016. Needle-free injection of 5-aminolevulinic acid in photodynamic therapy for the treatment of non-melanoma skin cancer. Dermatol. Ther. 29, 255–262. https://doi.org/10.1111/dth.12335.
Harris, F., Pierpoint, L., 2012. Photodynamic therapy based on 5-aminolevulinic acid and its use as an antimicrobial Agent. Med. Res. Rev. 32, 1292–1327. https://doi.org/10.1002/med.20251.
Li, X., Wang, X., Gu, J., Ma, Y., Liu, Z., Shi, Y., 2013. Needle-free injection of 5-aminolevulinic acid in photodynamic therapy for the treatment of condylomata acuminata. Exp. Ther. Med. 6, 236–240. https://doi.org/10.3892/etm.2013.1092.
Fargnoli, A.S., Katz, M.G., Williams, R.D., Kendle, A.P., Steuerwald, N., Bridges, C.R., 2016. Liquid jet delivery method featuring S100A1 gene therapy in the rodent model following acute myocardial infarction. Gene Ther. 23, 151–157. https://doi.org/10.1038/gt.2015.100.
Horiki, M., Yamato, E., Ikegami, H., Ogihara, T., Miyazaki, J., 2004. Needleless in vivo gene transfer into muscles by jet injection in combination with electroporation. J. Gene Med. 6, 1134–1138. https://doi.org/10.1002/jgm.612.
Kunugiza, Y., Tomita, N., Taniyama, Y., Tomita, T., Osako, M.K., Tamai, K., et al., 2006. Acceleration of wound healing by combined gene transfer of hepatocyte growth factor and prostacyclin synthase with Shima Jet. Gene Ther. 13, 1143–1152. https://doi.org/10.1038/sj.gt.3302767.
Sawamura, D., Ina, S., Itai, K., Meng, X., Kon, A., Tamai, K., et al., 1999. In vivo gene introduction into keratinocytes using jet injection. Gene Ther. 6, 1785. https://doi.org/10.1038/sj.gt.3301002.
Taniyama, Y., Azuma, J., Kunugiza, Y., Iekushi, K., Rakugi, H., Morishita, R., 2012. Therapeutic option of plasmid-DNA based gene transfer. Curr. Top. Med. Chem. 12, 1630–1637. https://doi.org/10.2174/156802612803531342.
Walther, W., Siegel, R., Kobelt, D., Knösel, T., Dietel, M., Bembenek, A., et al., 2008. Novel Jet-Injection Technology for Nonviral Intratumoral Gene Transfer in Patients with Melanoma and Breast Cancer. Clin. Cancer Res. 14, 7545–7553. https://doi.org/10.1158/1078-0432.CCR-08-0412.
Walther, W., Stein, U., Fichtner, I., Malcherek, L., Lemm, M., Schlag, P.M., 2001. Nonviral in vivo gene delivery into tumors using a novel low volume jet-injection technology. Gene Ther. 8, 173–180. https://doi.org/10.1038/sj.gt.3301350.
Barolet, D., Benohanian, A., 2018. Current trends in needle-free jet injection: an update. Clin. Cosmet. Investig. Dermatol. 11, 231–238. https://doi.org/10.2147/CCID.S162724.
Jones, A.T., Shen, X., Walter, K.L., LaBranche, C.C., Wyatt, L.S., Tomaras, G.D., et al., 2019. HIV-1 vaccination by needle-free oral injection induces strong mucosal immunity and protects against SHIV challenge. Nat. Commun. 10, 798. https://doi.org/10.1038/s41467-019-08739-4.
Arora, A., Hakim, I., Baxter, J., Rathnasingham, R., Srinivasan, R., Fletcher, D.A., et al., 2007. Needle-free delivery of macromolecules across the skin by nanoliter-volume pulsed microjets. Proc. Natl. Acad. Sci. USA 104, 4255–4260. https://doi.org/10.1073/pnas.0700182104.
Stachowiak, J.C., Li, T.H., Arora, A., Mitragotri, S., Fletcher, D.A., 2009. Dynamic control of needle-free jet injection. J. Controlled Release 135, 104–112. https://doi.org/10.1016/j.jconrel.2009.01.003.
Stachowiak, J.C., von Muhlen, M.G., Li, T.H., Jalilian, L., Parekh, S.H., Fletcher, D.A., 2007. Piezoelectric control of needle-free transdermal drug delivery. J. Controlled Release 124, 88–97. https://doi.org/10.1016/j.jconrel.2007.08.017.
McKeage, J.W., Ruddy, B.P., Nielsen, P.M.F., Taberner, A.J., 2018. Power-efficient controlled jet injection using a compound ampoule. J. Controlled Release 291, 127–134. https://doi.org/10.1016/j.jconrel.2018.10.025.
Taberner, A., Hogan, N.C., Hunter, I.W., 2012. Needle-free jet injection using real-time controlled linear Lorentz-force actuators. Med. Eng. Phys. 34, 1228–1235. https://doi.org/10.1016/j.medengphy.2011.12.010.
Fletcher, D.A., Palanker, D.V., 2001. Pulsed liquid microjet for microsurgery. Appl. Phys. Lett. 78, 1933–1935. https://doi.org/10.1063/1.1357452.
Avila, S.R.G., Song, C., Ohl, C.-D., 2015. Fast transient microjets induced by hemispherical cavitation bubbles. J. Fluid Mech. 767, 31–51. https://doi.org/10.1017/jfm.2015.33.
Chang, C., Sun, J., Hayashi, H., Suzuki, A., Sakaguchi, Y., Miyazaki, H., et al., 2019. Stable Immune Response Induced by Intradermal DNA Vaccination by a Novel Needleless Pyro-Drive Jet Injector. AAPS PharmSciTech 21, 19. https://doi.org/10.1208/s12249-019-1564-z.
Aran, K., Chooljian, M., Paredes, J., Rafi, M., Lee, K., Kim, A.Y., et al., 2017. An oral microjet vaccination system elicits antibody production in rabbits. Sci. Transl. Med. 9 https://doi.org/10.1126/scitranslmed.aaf6413.
Krizek, J., Goumoëns, F.D., Delrot, P., Moser, C., 2020. Needle-free delivery of fluids from compact laser-based jet injector. Lab Chip 20, 3784–3791. https://doi.org/10.1039/D0LC00646G.
Krizek, J., Delrot, P., Moser, C., 2020. Repetitive regime of highly focused liquid microjets for needle-free injection. Sci. Rep. 10, 5067. https://doi.org/10.1038/s41598-020-61924-0.
Han, T., Yoh, J.J., 2010. A laser based reusable microjet injector for transdermal drug delivery. J. Appl. Phys. 107, 103110 https://doi.org/10.1063/1.3430989.
Jang, H., Yu, H., Lee, S., Hur, E., Kim, Y., Lee, S.-H., et al., 2014. Towards clinical use of a laser-induced microjet system aimed at reliable and safe drug delivery. J. Biomed Opt. 19, 058001 https://doi.org/10.1117/1.JBO.19.5.058001.
Park, M., Jang, H., Sirotkin, F.V., Yoh, J.J., 2012. Er:YAG laser pulse for small-dose splashback-free microjet transdermal drug delivery. Opt. Lett. 37, 3894–3896. https://doi.org/10.1364/OL.37.003894.
Berrospe-Rodriguez, C., Visser, C.W., Schlautmann, S., Ramos-Garcia, R., Fernandez, R. D., 2016. Continuous-wave laser generated jets for needle free applications. Biomicrofluidics 10, 014104. https://doi.org/10.1063/1.4940038.
Oyarte Gálvez, L., Brió Pérez, M., Fernández, R.D., 2019. High speed imaging of solid needle and liquid micro-jet injections. J. Appl. Phys. 125, 144504 https://doi.org/10.1063/1.5074176.
Oyarte Gálvez, L., Fraters, A., Offerhaus, H.L., Versluis, M., Hunter, I.W., Fernández, R. D., 2020. Microfluidics control the ballistic energy of thermocavitation liquid jets for needle-free injections. J. Appl. Phys. 127, 104901 https://doi.org/10.1063/1.5140264.
Rodríguez, C.B., Visser, C.W., Schlautmann, S., Rivas, D.F., Ramos-García, R., 2017. Toward jet injection by continuous-wave laser cavitation. J. Biomed. Opt. 22, 105003 https://doi.org/10.1117/1.JBO.22.10.105003.
Tagawa, Y., Oudalov, N., El Ghalbzouri, A., Sun, C., Lohse, D., 2013. Needle-free injection into skin and soft matter with highly focused microjets. Lab Chip 13, 1357–1363. https://doi.org/10.1039/C2LC41204G.

Rohilla, P., Marston, J., 2020. Feasibility of laser induced jets in needle free jet injections. Int. J. Pharm. 589, 119714 https://doi.org/10.1016/j.ijpharm.2020.119714.
Moradiafrapoli, M., Marston, J.O., 2017. High-speed video investigation of jet dynamics from narrow orifices for needle-free injection. Chem. Eng. Res. Des. 117, 110–121. https://doi.org/10.1016/j.cherd.2016.10.023.
Shangguan, H., Casperson, L.W., Shearin, A., Gregory, K.W., Prahl, S.A., 1996. Drug delivery with microsecond laser pulses into gelatin. Appl. Opt. 35, 3347. https://doi.org/10.1364/AO.35.003347.
Vogel, A., Venugopalan, V., 2003. Mechanisms of Pulsed Laser Ablation of Biological Tissues. Chem. Rev. 103, 577–644. https://doi.org/10.1021/cr010379n.
Kiyama, A., Endo, N., Kawamoto, S., Katsuta, C., Oida, K., Tanaka, A., et al., 2019. Visualization of penetration of a high-speed focused microjet into gel and animal skin. J. Vis. https://doi.org/10.1007/s12650-019-00547-8.
Patakfalvi, L., Benohanian, A., 2014. Needle-free anaesthesia, a promising option for the needle-phobic patient. Br. J. Dermatol. 170, 1191–1192. https://doi.org/10.1111/bjd.12784.
Agostinis, P., Berg, K., Cengel, K.A., Foster, T.H., Girotti, A.W., Gollnick, S.O., et al., 2011. PHOTODYNAMIC THERAPY OF CANCER: AN UPDATE. CA Cancer J. Clin. 61, 250–281. https://doi.org/10.3322/caac.20114.
Tagawa, Y., Oudalov, N., Visser, C.W., Peters, I.R., van der Meer, D., Sun, C., et al., 2012. Highly Focused Supersonic Microjets. Phys. Rev. X 2, 031002. https://doi.org/10.1103/PhysRevX.2.031002.
Hale, G.M., Querry, M.R., 1973. Optical Constants of Water in the 200-nm to 200-μm Wavelength Region. Appl. Opt. 12, 555–563. https://doi.org/10.1364/AO.12.000555.
Keiser, G., Xiong, F., Cui, Y., Shum, P.P., 2014. Review of diverse optical fibers used in biomedical research and clinical practice. J. Biomed. Opt., 19, 080902. https://doi.org/10.1117/1.JBO.19.8.080902.
Frenz, M., Könz, F., Pratisto, H., Weber, H.P., Silenok, A.S., Konov, V.I., 1998. Starting mechanisms and dynamics of bubble formation induced by a Ho: Yttrium aluminum garnet laser in water. J. Appl. Phys. 84, 5905–5912. https://doi.org/10.1063/1.368906.
Paltauf, G., Schmidt-Kloiber, H., Frenz, M., 1998. Photoacoustic waves excited in liquids by fiber-transmitted laser pulses. J. Acoust. Soc. Am. 104, 890–897. https://doi.org/10.1121/1.423334.
Quinto-Su, P.A., Suzuki, M., Ohl, C.-D., 2014. Fast temperature measurement following single laser-induced cavitation inside a microfluidic gap. Sci. Rep. 4, 5445. https://doi.org/10.1038/srep05445.
Kattamis, N.T., McDaniel, N.D., Bernhard, S., Arnold, C.B., 2009. Laser direct write printing of sensitive and robust light emitting organic molecules. Appl. Phys. Lett. 94, 103306 https://doi.org/10.1063/1.3098375.
Jones, C.M., Henry, E.R., Hu, Y., Chan, C.K., Luck, S.D., Bhuyan, A., et al., 1993. Fast events in protein folding initiated by nanosecond laser photolysis. Proc. Natl. Acad. Sci. USA 90, 11860–11864.
Benedek, K., Walker, E., Doshier, L.A., Stout, R., 2005. Studies on the use of needle-free injection device on proteins. J. Chromatogr. A 1079, 397–407. https://doi.org/10.1016/j.chroma.2005.03.098.
Hogan, N.C., Hemond, B.D., Wendell, D.M., Taberner, A.J., Hunter, I.W., 2006. Delivery of Active Collagenase to Skin Using a Lorentz-Force Actuated Needle-Free Injector. 2006 Int. Conf. IEEE Eng. Med. Biol. Soc. 5611–5616. https://doi.org/10.1109/IEMBS.2006.260252.
Catanese, D.J., Fogg, J.M., Schrock, D.E., Gilbert, B.E., Zechiedrich, L., 2012. Supercoiled Minivector DNA resists shear forces associated with gene therapy delivery. Gene Ther. 19, 94–100. https://doi.org/10.1038/gt.2011.77.
Walther, W., Stein, U., Fichtner, I., Voss, C., Schmidt, T., Schleef, M., et al., 2002. Intratumoral low-volume jet-injection for efficient nonviral gene transfer. Mol. Biotechnol. 21, 105–115.
Cartier, R., Ren, S.V., Walther, W., Stein, U., Lewis, A., Schlag, P.M., et al., 2000. In Vivo Gene Transfer by Low-Volume Jet Injection. Anal. Biochem. 282, 262–265. https://doi.org/10.1006/abio.2000.4619.
Walther, W., Stein, U., Fichtner, I., Kobelt, D., Aumann, J., Arlt, F., et al., 2005. Nonviral Jet-Injection Gene Transfer for Efficient in Vivo Cytosine Deaminase Suicide Gene Therapy of Colon Carcinoma. Mol. Ther. 12, 1176–1184. https://doi.org/10.1016/j.ymthe.2005.07.700.
Peters, I.R., Tagawa, Y., Oudalov, N., Sun, C., Prosperetti, A., Lohse, D., et al., 2013. Highly focused supersonic microjets: numerical simulations. J. Fluid Mech. 719, 587–605. https://doi.org/10.1017/jfm.2013.26.
Paltauf, G., Schmidt-Kloiber, H., 1996. Microcavity dynamics during laser-induced spallation of liquids and gels. Appl. Phys. A 62, 9.
Fargnoli, A.S., Katz, M.G., Williams, R.D., Margulies, K.B., Bridges, C.R., 2014. A Needleless Liquid Jet Injection Delivery Method for Cardiac Gene Therapy: a Comparative Evaluation Versus Standard Routes of Delivery Reveals Enhanced Therapeutic Retention and Cardiac Specific Gene Expression. J. Cardiovasc. Transl. Res. 7, 756–767. https://doi.org/10.1007/s12265-014-9593-1.
Delrot, P., Modestino, M.A., Gallaire, F., Psaltis, D., Moser, C., 2016. Inkjet Printing of Viscous Monodisperse Microdroplets by Laser-Induced Flow Focusing. Phys. Rev. Appl. 6, 024003 https://doi.org/10.1103/PhysRevApplied.6.024003.
Niederholtmeyer, H., Sun, Z.Z., Hori, Y., Yeung, E., Verpoorte, A., Murray, R.M., et al., 2015. Rapid cell-free forward engineering of novel genetic ring oscillators. ELife 4, e09771. https://doi.org/10.7554/eLife.09771.
Lavickova, B., Maerkl, S.J., 2019. A Simple, Robust, and Low-Cost Method To Produce the PURE Cell-Free System. ACS Synth. Biol. 8, 455–462. https://doi.org/10.1021/acssynbio.8b00427.
Maggio, R.M., Calvo, N.L., Vignaduzzo, S.E., Kaufman, T.S., 2014. Pharmaceutical impurities and degradation products: Uses and applications of NMR techniques. J. Pharm. Biomed. Anal. 101, 102–122. https://doi.org/10.1016/j.jpba.2014.04.016.
Elfsson, B., Wallin, I., Eksborg, S., Rudaeus, K., Ros, A.M., Ehrsson, H., 1999. Stability of 5-aminolevulinic acid in aqueous solution. Eur. J. Pharm. Sci. 7, 87–91. https://doi.org/10.1016/S0928-0987(98)00009-8.
Bunke, A., Zerbe, O., Schmid, H., Burmeister, G., Merkle, H.P., Gander, B., 2000. Degradation mechanism and stability of 5-aminolevulinic acid. J. Pharm. Sci. 89, 1335–1341. https://doi.org/10.1002/1520-6017(200010)89:10<1335::aid-jps11>3.0.co;2-#.
Kadioglu, Y., Atila, A., Serdar Gultekin, M., Alcan, Alp N., 2013. Investigation of Behavior of Forced Degradation of Lidocaine HCl by NMR Spectroscopy and GC-FID Methods: Validation of GC-FID Method for Determination of Related Substance in Pharmaceutical Formulations. Iran J. Pharm. Res. IJPR 12, 659–669.
Dunbar, C.E., High, K.A., Joung, J.K., Kohn, D.B., Ozawa, K., Sadelain, M., 2018. Gene therapy comes of age. Science 359. https://doi.org/10.1126/science.aan4672.
Sarker, S.R., Ball, A.S., Bhargava, S.K., Soni, S.K., 2019. Evaluation of plasmid DNA stability against ultrasonic shear stress and its *in vitro* delivery efficiency using ionic liquid [Bmim][PF_6]. RSC Adv. 9, 29225–29231. https://doi.org/10.1039/C9RA03414E.
Wu, Z., Zhan, S., Fan, W., Ding, X., Wu, X., Zhang, W., et al., 2016. Peptide-Mediated Tumor Targeting by a Degradable Nano Gene Delivery Vector Based on Pluronic-Modified Polyethylenimine. Nanoscale Res. Lett. 11, 122. https://doi.org/10.1186/s11671-016-1337-5.
Nguyen, T.H., Elimelech, M., 2007. Adsorption of Plasmid DNA to a Natural Organic Matter-Coated Silica Surface: Kinetics, Conformation, and Reversibility. Langmuir 23, 3273–3279. https://doi.org/10.1021/la0622525.
Lentz, Y.K., Worden, L.R., Anchordoquy, T.J., Lengsfeld, C.S., 2005. Effect of jet nebulization on DNA: identifying the dominant degradation mechanism and mitigation methods. J. Aerosol. Sci. 36, 973–990. https://doi.org/10.1016/j.jaerosci.2004.11.017.